J Electr Eng Technol Vol. 9, No. 1: 60-70, 2014
http://dx.doi.org/10.5370/JEET.2014.9.1.060

ISSN(Print) 1975-0102
ISSN(Online) 2093-7423

Effects of Wind Generation Uncertainty and Volatility on Power System Small Signal Stability

Li-Bao Shi†, Li Kang*, Liang-Zhong Yao, Shi-Yao Qin**, Rui-Ming Wang** and Jin-Ping Zhang****

Abstract – This paper discusses the impacts of large scale grid-connected wind farm equipped with permanent magnet synchronous generator (PMSG) on power system small signal stability (SSS) incorporating wind generation uncertainty and volatility. Firstly, a practical simplified PMSG model with rotor-flux-oriented control strategy applied is derived. In modeling PMSG generator side converter, the generator-voltage-oriented control strategy is utilized to implement the decoupled control of active and reactive power output. In modeling PMSG grid side converter, the grid-voltage-oriented control strategy is applied to realize the control of DC link voltage and the reactive power regulation. Based on the Weibull distribution of wind speed, the Monte Carlo simulation technique based is carried out on the IEEE 16-generator-68-bus test system as benchmark to study the impacts of wind generation uncertainty and volatility on small signal stability. Finally, some preliminary conclusions and comments are given.

Keywords: Wind power, PMSG, Small signal stability, Electromechanical oscillations, Uncertainty and volatility

1. Introduction

Currently, the greenhouse effect and the energy crisis are seriously threatening the sustainable development of the human society. To tackle the intractable issue effectively, it is imperative to find new energy resources to replace the traditional fossil fuels. The good news is that more and more countries in the world are increasingly concerned about the development and utilization of renewable energy resources. As one of the renewable energy sources with the most mature technology and the largest application scale, wind power has been gaining more and more attention in virtue of its great contributions in reducing environmental pollution and adjusting the energy structure. Comparing with the traditional power generation technologies, the wind power is characterized with a nature of uncertainty and volatility. With a high penetration of wind power, how to systematically and effectively assess the impacts of intermittent wind power on power system dynamics, especially on the small signal stability (SSS) becomes one of the most challenging cutting-edge issues to be solved in exploring and exploiting large-scale wind power integration.

So far, much existing work corresponding to the impacts of wind power on the dynamic behavior of the power system mainly focused on the doubly-fed induction generator (DFIG) [1] which is currently widely used in wind farms. F. Mei et al [2] described the modeling and small signal analysis of a grid connected doubly-fed induction generator. The DFIG electromechanical models were analyzed by the eigenvalues and participation factor. F. Wu et al [3] derived the small signal stability model based on the DFIG and its control system. A conclusion with the improvement of damping characteristics when integrating wind farm of DFIG type was drawn. V. Vittal et al [4] proposed a comprehensive framework based on eigenvalue sensitivity to examine the effect of penetration of DFIGs on a large system. The case studies were carried out under the simulation environment DSATools developed by PowerTech Labs, Inc. Shi L. et al [5] discussed the impacts of wind power intermittency on power system small signal stability. The Monte Carlo technique was applied to reveal how the grid-connected wind farm of DFIG type affects the small signal stability of an existing power system. Comparing with DFIG, the direct-driven permanent magnet synchronous generator (PMSG) is considered as an important alternative in the future development of wind power due to its higher generation efficiency, gearless structure, lower maintenance cost and higher operation reliability. Espen H. et al [6] investigated the impacts of wind power integration in Norway on the damping of inter-area mode oscillations. Several types of wind generators involving direct drive synchronous generator were tested during simulations. Wu F. et al [7] presented a model of direct-drive permanent magnet generator (DDPMG) and its controllers. The corresponding small signal stability was carried out to show that the

† Corresponding Author: National Key Laboratory of Power System in Shenzhen, Graduate School at Shenzhen, Tsinghua University, China. (shilb@sz.tsinghua.edu.cn)
* National Key Laboratory of Power System in Shenzhen, Graduate School at Shenzhen, Tsinghua University, China.
** China Electric Power Research Institute, Qinghe, Beijing, China. (yaoliangzhong@epri.sgcc.com.cn)
Received: June 21, 2013; Accepted: August 30, 2013

controller can improve the small signal stability of the wind turbine system. Kang L. et al [8] studied the impacts of grid-connected wind farm of direct-driven PMSG type on power system small signal stability. A simplified practical model of PMSG was derived. The IEEE 3-generator-9-bus system was tested to conduct the eigenvalue analysis. T. Knuppel et al [9] assessed the impact of full-load converter interfaced wind turbines on small signal stability. The effects of selected wind turbine and wind farm control parameters were studied based on sensitivity analysis. S. Q. Bu et al [10] proposed a method which can directly calculate the probabilistic density function of critical eigenvalues to investigate the impacts of wind generation uncertainty on small signal stability. H. Huang et al [11] built a small signal simulation model under MATLAB/SIMULINK environment to study the stability of grid-connected wind farm equipped with direct drive permanent magnet synchronous generator. H. Z. Huang et al [12] investigated the effects of plug-in electric vehicles and wind farm of DFIG type on power system small signal stability via applying quasi-Monte Carlo method. Compared to the conventional Monte Carlo simulation, more reliable results with shorter computational efforts can be obtained. M. Jafarian et al [13] developed a method to study the interaction of the dynamics of wind farm of DFIG type with the synchronous generators. The proposed method was based on the sensitivity of synchronous generators electromechanical eigenvalue with respect to variations in Jacobian matrix. It should be noted that the existing achievements in exploring and exploiting the impacts of wind power integration on power system SSS mainly focus on the deterministic evaluation, i.e. the nature of wind power uncertainty and volatility is rarely involved in evaluating the effects of wind generation integration on the dynamic behavior of power systems.

In this paper, a simplified practical model of PMSG and its associated controllers is derived. The Monte Carlo method based on the Weibull distribution of wind speed is applied in the solutions of IEEE 16-generator-68-bus test system as benchmark to reveal the impacts of grid-connected wind farm of PMSG type on power system SSS incorporating wind generation uncertainty and volatility.

This paper is organized as follows. Section 2 details the dynamic model of PMSG. In Section 3 a framework for the SSS evaluation incorporating wind power uncertainty based on Monte Carlo simulation is discussed. The case studies are given in Section 4. Finally, the conclusions are summarized in Section 5.

2. PMSG Modeling

In this section, a simplified practical electromechanical (EM) model of wind farm equipped with PMSG is derived elaborately. A general configuration of a PMSG including the power electronic converters and controllers is depicted in Fig. 1. The PMSG is connected to the power grid through a back-to-back power electronic converter.

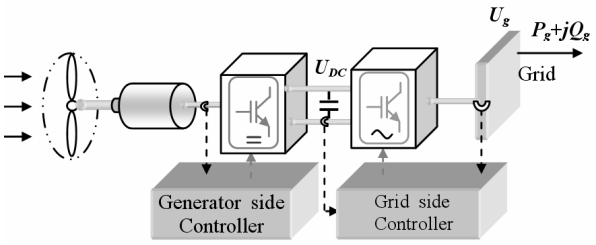

Fig. 1. Typical PMSG configuration

2.1 PMSG model

In order to build the dynamic mathematical model of PMSG in d-q axis, the following assumptions are given during analysis: (i) Magnetic saturation effects are negligible; (ii) Eddy current loss and magnetic hysteresis loss are negligible; (iii) One-mass or lumped model is applied for the wind turbine drive train systems; (iv) Stator transients and stator resistance are negligible. With these assumptions mentioned above, and by applying the rotor-flux-oriented control technique [7] in modeling PMSG, we have

$$u_{ds} = \omega_e L_q i_{qs} \tag{1}$$

$$u_{qs} = \omega_e \psi_f - \omega_e L_d i_{ds} \tag{2}$$

where u_{ds}, u_{qs}, i_{ds} and i_{qs} are stator voltage and stator current in d-q axis, respectively; L_d and L_q are the sta tor inductance in d-q axis, respectively; ψ_f is the mag net flux linkage; ω_e is generator electrical speed.

The active and reactive power outputs of the wind turbine generator (WTG) are given by

$$P_s = u_{ds} i_{ds} + u_{qs} i_{qs} \tag{3}$$

$$Q_s = u_{qs} i_{ds} - u_{ds} i_{qs} \tag{4}$$

The corresponding swing equation is as

$$2H \frac{d\omega_e}{dt} + D(\omega_e - 1) = T_m - T_e \tag{5}$$

$$\frac{d\delta}{dt} = \omega_B(\omega_e - 1) \tag{6}$$

where H is the inertia constant; D is the damping coefficient; T_m and T_e are the mechanical and generator electromagnetic torque, respectively; δ is defined as the angle in which q-axis leads x-axis. ω_B is the speed base.

2.2 Converter model

The converter system consists of generator side

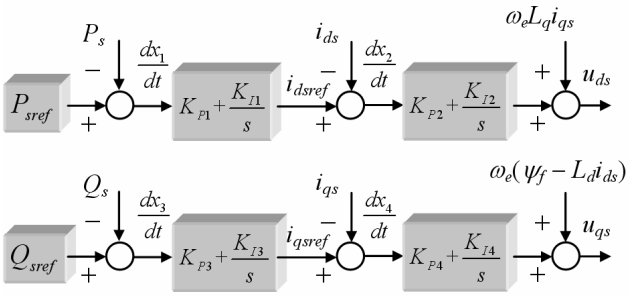

Fig. 2. Control block diagram of generator side converter

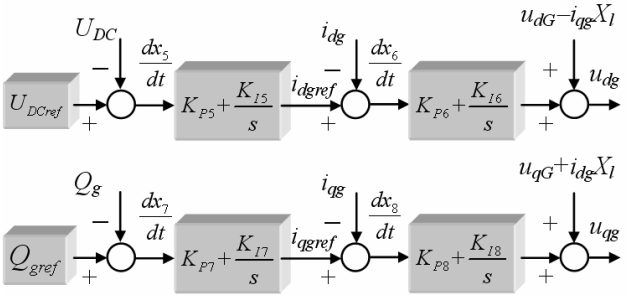

Fig. 3. Control block diagram of grid side converter

converter, grid side converter, DC link and converter control. In normal operation, there is no reactive power exchange between generator side and grid side converter. Only active power is delivered by the generator side converter to the grid side converter. With the power losses of generator side and grid side converter neglected, the model of the DC link can be derived as

$$CU_{DC}\frac{dU_{DC}}{dt} = (u_{ds}i_{ds} + u_{qs}i_{qs}) - (u_{dg}i_{dg} + u_{qg}i_{qg}) \tag{7}$$

where C is the capacitor of the DC link; U_{DC} is the voltage of C; u_{dg}, u_{qg}, i_{dg} and i_{qg} are grid side converter voltage and current feeding the grid in d-q axis.

Fig. 2 illustrates the control block diagram of generator side converter, which is utilized to control the active and reactive power of PMSG.

Based on the generator-voltage-oriented control strategy [8], the corresponding state equations can be derived below

$$\frac{dx_1}{dt} = P_{ref} - P_s \tag{8}$$

$$i_{dsref} = K_{P1}(P_{ref} - P_s) + K_{I1}x_1 \tag{9}$$

$$\frac{dx_2}{dt} = i_{dsref} - i_{ds} = K_{P1}(P_{ref} - P_s) + K_{I1}x_1 - i_{ds} \tag{10}$$

$$\frac{dx_3}{dt} = Q_{ref} - Q_s \tag{11}$$

$$i_{qsref} = K_{P3}(Q_{ref} - Q_s) + K_{I3}x_3 \tag{12}$$

$$\frac{dx_4}{dt} = i_{qsref} - i_{qs} = K_{P3}(Q_{ref} - Q_s) + K_{I3}x_3 - i_{qs} \tag{13}$$

$$u_{ds} = K_{P2}(K_{P1}(P_{ref} - P_s) + K_{I1}x_1 - i_{ds}) + K_{I2}x_2 + \omega_e L_q i_{qs} \tag{14}$$

$$\begin{aligned} u_{qs} = {} & K_{P4}(K_{P3}(Q_{ref} - Q_s) + K_{I3}x_3 - i_{qs}) \\ & + K_{I4}x_4 + \omega_e\psi_f - \omega_e L_d i_{ds} \end{aligned} \tag{15}$$

where K_{P1}, K_{P2}, K_{P3}, K_{P4}, K_{I1}, K_{I2}, K_{I3} and K_{I4} are the PI controller gain and time constants respectively. x_1, x_2 ,x_3, x_4 are the introduced intermediate variables; P_{ref}, Q_{ref} are the active power and reactive power control reference values, respectively; i_{dsref}, i_{qsref} are the specified d-axis and q-axis stator current reference values, respectively.

Fig. 3 illustrates the control block diagram of grid side converter, which is utilized to maintain the DC link voltage and control the reactive power exchange between the generator side and grid side converter.

Based on the grid-voltage-oriented control strategy [8], the corresponding state equations can be derived below

$$\frac{dx_5}{dt} = U_{DCref} - U_{DC} \tag{16}$$

$$i_{dgref} = K_{P5}(U_{DCref} - U_{DC}) + K_{I5}x_5 \tag{17}$$

$$\frac{dx_6}{dt} = i_{dgref} - i_{dg} = K_{P5}(U_{DCref} - U_{DC}) + K_{I5}x_5 - i_{dg} \tag{18}$$

$$\frac{dx_7}{dt} = Q_{gref} - Q_g \tag{19}$$

$$i_{qgref} = K_{P7}(Q_{gref} - Q_g) + K_{I7}x_7 \tag{20}$$

$$\frac{dx_8}{dt} = i_{qgref} - i_{qg} = K_{P7}(Q_{gref} - Q_g) + K_{I7}x_7 - i_{qg} \tag{21}$$

$$\begin{aligned} u_{dg} = {} & K_{P6}(K_{P5}(U_{DCref} - U_{DC}) + K_{I5}x_5 - i_{dg}) \\ & + K_{I6}x_6 + u_{dG} - i_{qg}X_l \end{aligned} \tag{22}$$

$$\begin{aligned} u_{qg} = {} & K_{P8}(K_{P7}(Q_{gref} - Q_g) + K_{I7}x_7 - i_{qg}) \\ & + K_{I8}x_8 + u_{qG} + i_{dg}X_l \end{aligned} \tag{23}$$

where K_{P5}, K_{P6}, K_{P7}, K_{P8}, K_{I5}, K_{I6}, K_{I7} and K_{I8} are the PI controller gain and time constants respectively. x_5, x_6, x_7, x_8 are the introduced intermediate variables; Q_{gref} is the reference value of the reactive power of the grid; i_{dgref}, i_{qgref} are the specified d-axis and q-axis grid current reference values, respectively.

Eqs.(1-23) constitute the 11th order simplified practical electromechanical model of a PMSG system.

2.3 Wind farm model

It is known that a large wind farm consists of tens or hundreds of WTGs. It is different for each WTG to capture the wind energy from the incoming wind due to the wake effect [14]. In general, the details how to take wake effect into account for the whole wind farm are negligible during the system impact studies. The corresponding simplifications and assumptions are imperative.

In this paper, one equivalent single WTG model [15] representing the entire wind farm is employed to

implement the modeling of wind farm.

2.4 Wind turbine model

The following functions approximation [1] with maximum power point tracking (MPPT) control strategy is widely used to model wind turbine.

$$P_m=\begin{cases}0 & v_w \le v_{cut-in} \ or \ v_w \ge v_{cut-off}\\ 0.5\rho AC_{p\max}(\beta,\lambda_{opt})v_w^3 & v_{cut-in} < v_w \le v_{rated}\\ P_r & v_{rated} < v_w < v_{cut-off}\end{cases} \quad (24)$$

where v_w is the wind speed; P_m is the power output of the wind turbine; ρ is the air density (kg/m^3); A is the area covered by the wind turbine rotor (m^2); $C_{p\max}$ is the optimal power coefficient; β is the blade pitch angle; λ_{opt} is the optimal tip-speed ratio; $v_{cut\text{-}in}$ and $v_{cut\text{-}off}$ are the cut-in and cut-off wind speed, respectively; v_{rated} is the rated wind speed at which the power output of wind turbine will be the rated power.

Eq.(24) denotes the relationship between wind speed and the mechanical power extracted from the wind.

3. Monte Carlo Simulation Based SSS Evaluation Incorporating Wind Power Volatility

3.1 SSS evaluation incorporating wind farm of PMSG type

SSS is defined as the ability to maintain synchronism when subjected to small disturbances [16]. In accordance with the SSS theory, for a dynamic autonomous power system described by a set of non-linear ordinary differential and algebraic equations, the corresponding state matrix with appropriate linearization treatment can by derived as

$$\mathbf{\Lambda = A - BD^{-1}C} \quad (25)$$

where $\mathbf{\Lambda}$ is called as the state matrix; **A**, **B**, **C** and **D** are the Jacobian matrices of the test system.

The corresponding eigenvalues and eigenvectors of $\mathbf{\Lambda}$ can denote the stability of the test system at a specific operating condition.

For a power system with integration of wind farm equipped with PMSG, the deduction of state matrix can be briefly described as follows. According to the aforementioned derived 11th order simplified model of PMSG system, the state variables are ω_e, δ, x_1, x_2, x_3, x_4, U_{DC}, x_5, x_6, x_7 and x_8, respectively; the algebraic variables are u_{ds}, u_{qs}, u_{dg}, u_{qg}, i_{ds}, i_{qs}, i_{dg} and i_{qg}, respectively. Then the corresponding Jacobian matrices $\mathbf{A_{pmsg}}$, $\mathbf{B_{pmsg}}$, $\mathbf{C_{pmsg}}$ and $\mathbf{D_{pmsg}}$ can be derived as

$$\frac{d\mathbf{\Delta x}}{dt} = \mathbf{A_{pmsg}\Delta x + B_{pmsg}\Delta I_{dq}} \quad (26)$$

$$\mathbf{\Delta U_{dq} = C_{pmsg}\Delta x + D_{pmsg}\Delta I_{dq}} \quad (27)$$

Where

$$\mathbf{A_{pmsg}}=\begin{array}{c}\begin{matrix}\Delta\omega_e & \Delta\delta & \Delta x_1 & \Delta x_2 & \Delta x_3 & \Delta x_4 & \Delta U_{DC} & \Delta x_5 & \Delta x_6 & \Delta x_7 & \Delta x_8\end{matrix}\\ \begin{bmatrix} a_{11} & 0 & a_{13} & a_{14} & a_{15} & a_{16} & 0 & 0 & 0 & 0 & 0\\ a_{21} & 0 & 0 & 0 & 0 & 0 & 0 & 0 & 0 & 0 & 0\\ a_{31} & 0 & a_{33} & a_{34} & a_{35} & a_{36} & 0 & 0 & 0 & 0 & 0\\ a_{41} & 0 & a_{43} & a_{44} & a_{45} & a_{46} & 0 & 0 & 0 & 0 & 0\\ a_{51} & 0 & a_{53} & a_{54} & a_{55} & a_{56} & 0 & 0 & 0 & 0 & 0\\ a_{61} & 0 & a_{63} & a_{64} & a_{65} & a_{66} & 0 & 0 & 0 & 0 & 0\\ a_{71} & 0 & a_{73} & a_{74} & a_{75} & a_{76} & a_{77} & a_{78} & a_{79} & a_{710} & a_{711}\\ 0 & 0 & 0 & 0 & 0 & 0 & 1 & 0 & 0 & 0 & 0\\ 0 & 0 & 0 & 0 & 0 & 0 & a_{97} & a_{98} & 0 & 0 & 0\\ 0 & 0 & 0 & 0 & 0 & 0 & a_{107} & a_{108} & a_{109} & a_{1010} & a_{1011}\\ 0 & 0 & 0 & 0 & 0 & 0 & a_{117} & a_{118} & a_{119} & a_{1110} & a_{1111}\end{bmatrix}\end{array}$$

$$\mathbf{C_{pmsg}}=\begin{bmatrix} c_1 & 0 & c_2 & c_3 & c_4 & c_5 & 0 & 0 & 0 & 0 & 0\\ d_1 & 0 & d_2 & d_3 & d_4 & d_5 & 0 & 0 & 0 & 0 & 0\\ 0 & 0 & 0 & 0 & 0 & 0 & a_1 & a_2 & a_3 & 0 & 0\\ 0 & 0 & 0 & 0 & 0 & 0 & b_1 & b_2 & b_3 & b_4 & b_5\end{bmatrix}$$

$$\mathbf{B_{pmsg}}=\begin{array}{c}\begin{matrix}\Delta i_{ds} & \Delta i_{qs} & \Delta i_{dg} & \Delta i_{qg}\end{matrix}\\ \begin{bmatrix} b_{11} & b_{12} & 0 & 0\\ 0 & 0 & 0 & 0\\ b_{31} & b_{32} & 0 & 0\\ b_{41} & b_{42} & 0 & 0\\ b_{51} & b_{52} & 0 & 0\\ b_{61} & b_{62} & 0 & 0\\ b_{71} & b_{72} & b_{73} & b_{74}\\ 0 & 0 & 0 & 0\\ 0 & 0 & b_{93} & 0\\ 0 & 0 & b_{103} & b_{104}\\ 0 & 0 & b_{113} & b_{114}\end{bmatrix}\end{array} \quad \mathbf{D_{pmsg}}=\begin{bmatrix} c_6 & c_7 & 0 & 0\\ d_6 & d_7 & 0 & 0\\ 0 & 0 & a_4 & a_5\\ 0 & 0 & b_6 & b_7\end{bmatrix}$$

By transforming the algebraic variables in d-q coordinate system to the synchronous rotating coordinate system (also called as x-y coordinate system), we have

$$\frac{d\mathbf{\Delta x}}{dt} = \mathbf{A_{WF}\Delta x + B_{WF}\Delta U_{xy}} \quad (28)$$

$$0 = \mathbf{C_{WF}\Delta x + D_{WF}\Delta U_{xy}} \quad (29)$$

where $\mathbf{A_{WF}}=\mathbf{A_{pmsg}}$; $\mathbf{B_{WF}}=\mathbf{B_{pmsg}TY_{WFWF}}$; $\mathbf{C_{WF}}=\mathbf{-T^{-1}C_{pmsg}}$;

$\mathbf{D_{WF}}=\mathbf{I_{4\times4}}-\mathbf{T^{-1}D_{pmsg}TY_{WFWF}}$

$$\mathbf{T}=\begin{bmatrix}\sin\delta & -\cos\delta\\ \cos\delta & \sin\delta\end{bmatrix};\quad \mathbf{Y_{WFWF}}=\begin{bmatrix}\mathbf{Y_{dqs}} & \\ & \mathbf{Y_{GmGm}}\end{bmatrix}$$

Assume that a power system consists of n generators (wind farm involved as well as traditional synchronous generators) and N buses with m state variables. By eliminating $\mathbf{\Delta U_{xy}}$ descried in (27) and (28), finally we can obtain the system state matrix as given below

$$\mathbf{\Lambda = A - BD^{-1}C} \tag{30}$$

where $\mathbf{A}=\left[\mathbf{A_G}\right]_{m\times m}$; $\mathbf{B}=\left[\mathbf{B_G}\ \mathbf{0}\right]_{m\times 2N}$;

$$\mathbf{C}=\begin{bmatrix}\mathbf{-C_G}\\ \mathbf{0}\end{bmatrix}_{2N\times m};\quad \mathbf{D}=\begin{bmatrix}\mathbf{Y_{GG}-D_G} & \mathbf{Y_{GL}}\\ \mathbf{Y_{LG}} & \mathbf{Y_{LL}}\end{bmatrix}_{2N\times 2N}$$

$$\mathbf{A_G}=\begin{bmatrix}\mathbf{A_{G1}} & & & \\ & \cdots & & \\ & & \mathbf{A_{WF}} & \\ & & & \cdots \\ & & & \mathbf{A_{Gn}}\end{bmatrix}_{m\times m}\quad \mathbf{B_G}=\begin{bmatrix}\mathbf{B_{G1}} & & & \\ & \cdots & & \\ & & \mathbf{B_{WF}} & \\ & & & \cdots \\ & & & \mathbf{B_{Gn}}\end{bmatrix}_{m\times 2N}$$

$$\mathbf{C_G}=\begin{bmatrix}\mathbf{C_{G1}} & & & \\ & \cdots & & \\ & & \mathbf{-C_{WF}} & \\ & & & \cdots \\ & & & \mathbf{C_{Gn}}\end{bmatrix}_{2N\times m}\quad \mathbf{D_G}=\begin{bmatrix}\mathbf{D_{G1}} & & & \\ & \cdots & & \\ & & \mathbf{Y_{GG}-D_{WF}} & \\ & & & \cdots \\ & & & \mathbf{D_{Gn}}\end{bmatrix}_{2N\times 2N}$$

3.2 Monte carlo based SSS evaluation incorporating wind power volatility

In order to simulate and study the impacts of wind power uncertainty and volatility on SSS more accurately and systematically, the Monte Carlo simulation technique is applied during analysis. In our work, the following Weibull distribution [17] is employed to describe the uncertainties of wind speed v_w, the source of causing wind power uncertainty and volatility.

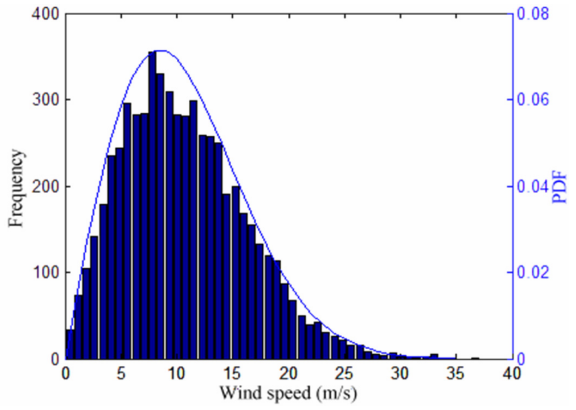

Fig. 4. Weibull distribution of wind speed (k=2, c=12m/s) and frequency distribution based on Monte Carlo method

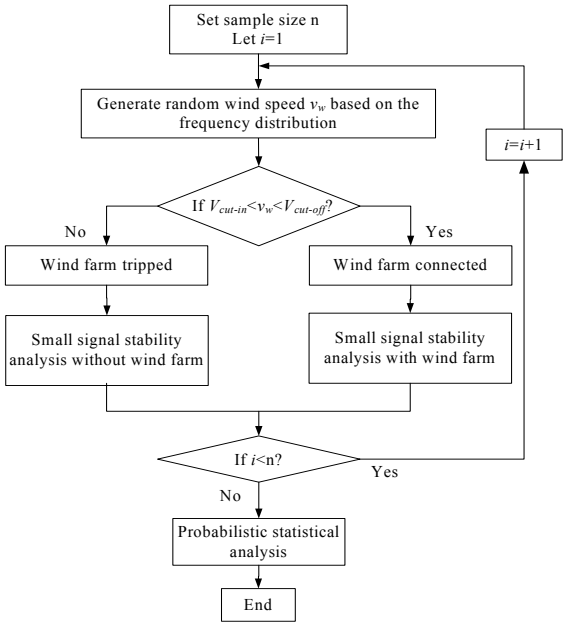

Fig. 5. Flow chart of SSS analysis incorporating wind power based on Monte Carlo method

$$f(v_w)=kc^{-k}v_w^{k-1}\exp(-v_w/c)^k \tag{31}$$

where k and c denote the shape and scale parameter, respectively. In this paper, the Weibull distribution with k=2 and c=12m/s as shown in Fig. 4 are selected as the probability distribution of regional wind speed. The sample size n is set to be 6000.

The main procedures of implementing SSS evaluation with wind farm involved based on Monte Carlo simulation are as follows

(i) Set the total sample size for Monte Carlo simulation;
(ii) Generate a random wind speed v_w in terms of frequency distribution of wind speed, and verify if wind farm can be connected to power grid in accordance with the grid-connected condition ($v_{cut\text{-}in}<v_w<v_{cut\text{-}off}$);
(iii) If the grid-connected condition is not satisfied, i.e. $v_w \le v_{cut\text{-}in}$ or $v_w \ge v_{vcut\text{-}off}$, to conduct the SSS evaluation without wind farm integration; otherwise to conduct the SSS evaluation incorporating wind power;
(iv) Repeat (ii) and (iii) until the pre-set sample size is reached;
(v) Make probabilistic statistical analysis based on the simulation results to reveal the impacts of wind power uncertainty and volatility on SSS.

The flow chart of SSS analysis incorporating wind power based on Monte Carlo method is given in Fig. 5.

4. Application Example

The 16-generator-68-bus test system [18] as shown in Fig. 6 is employed to assess the effects of wind generation uncertainty and volatility on SSS. In this system, generator G13 (slack bus) is modeled as the classic model; the remaining generators are modeled as the 4th order model with a simplified 3rd order excitation system model. Two simulation scenarios are designed below for the simulation studies: (i) In scenario 1, the wind farm equipped with PMSGs substitutes for the traditional synchronous generator; (ii) In scenario 2, the wind farm is connected to a load bus directly. Furthermore, the wind farm equipped with DFIGs modeled as a 7th order simplified model [5] is also introduced for comparisons during simulations. The details of DFIG modeling and corresponding parameters can be found in [5]. The parameters of PMSG are given in Table 1. The optimized parameters of PI controllers shown in Fig. 2 and Fig. 3 are given in Table 2 and Table 3 with respect to different scenarios. All simulations are executed under the MATLAB™ environment.

Table 1. Parameters of PMSG

Item	Value
Air density ρ (kg/m^3)	1.2235
Radius of rotor R (m)	60
Cut-in wind speed $v_{cut\text{-}in}$ (m/s)	3
Cut-off wind speed $v_{cut\text{-}off}$ (m/s)	30
Rated wind speed v_{rated} (m/s)	11.52
Rated power P_r (MW)	5
Rated line voltage U_r (kV)	1.0
Number of pole pairs p	75
Inertia constant H (sec)	3
Frequency f (Hz)	50
Stator resistance R_s (pu)	0.01
d-axis reactance X_d (pu)	1.0
q-axis reactance X_q (pu)	0.7
Field flux ψ_f (pu)	1.55
DC capacitor C (pu)	0.55
Line reactance X_l (pu)	0.4

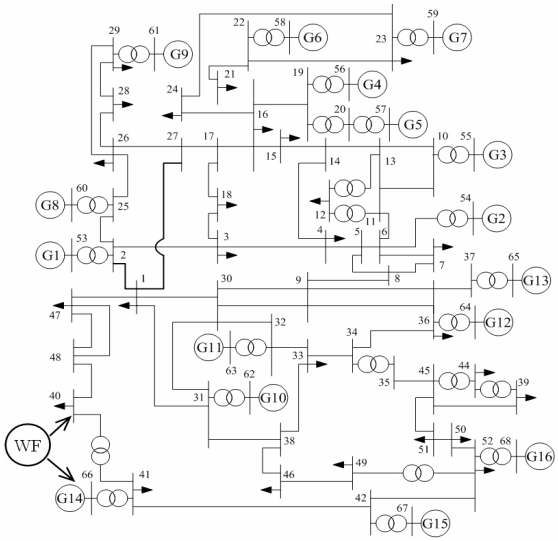

Fig. 6. IEEE 16-generator-68-bus test system

Table 2. Parameters of PI controllers applied in scenario 1

Item	Value(p.u.)	Item	Value(p.u.)
K_{P1}	8.54	K_{P5}	300
K_{I1}	259.24	K_{I5}	0.001
K_{P2}	300	K_{P6}	0.001
K_{I2}	0.001	K_{I6}	0.001
K_{P3}	197.01	K_{P7}	0.001
K_{I3}	117.68	K_{I7}	152.97
K_{P4}	300	K_{P8}	0.001
K_{I4}	0.001	K_{I8}	300

Table 3. Parameters of PI controllers applied in scenario 2

Item	Value(p.u.)	Item	Value(p.u.)
K_{P1}	0.001	K_{P5}	0.001
K_{I1}	200	K_{I5}	0.001
K_{P2}	0.001	K_{P6}	135.25
K_{I2}	0.001	K_{I6}	0.001
K_{P3}	104.16	K_{P7}	2
K_{I3}	82	K_{I7}	0.001
K_{P4}	0.001	K_{P8}	200
K_{I4}	200	K_{I8}	0.001

4.1 Scenario 1: Replacing synchronous generator

Firstly, the wind farms equipped with PMSGs and DFIGs substitute for all the synchronous generators except the reference machine G13, respectively. We found after the initial simulations that when the wind farm of PMSG type substitutes for the traditional synchronous generators G14 and G16, the test system keeps stable. When substituting for the remaining synchronous generators, the test system is unstable. When the wind farm of DFIG type substitutes for the synchronous generators G2-G4, G7 and G12, the test system is small signal stable. Furthermore, the simulation results show that whatever the wind farm of PMSG type or DFIG type is integrated into the power grid, they all do not participate in the EM oscillations. Table 4 gives the obtained EM oscillatory modes and their

Table 4. The EM oscillatory properties when substituting for G16 in scenario 1

No.	G16 replaced by PMSG		G16 replaced by DFIG	
	Damping ratio	Oscillation frequency	Damping ratio	Oscillation frequency
EM1	0.0354	1.7013	0.0321	1.8560
EM2	0.0629	1.3849	0.0596	1.5217
EM3	0.0789	1.3861	0.0746	1.5233
EM4	0.0979	1.3568	0.0928	1.4946
EM5	0.0451	1.2231	0.0424	1.3409
EM6	0.0402	1.1724	0.0362	1.2835
EM7	0.0540	1.1543	0.0495	1.2659
EM8	0.0857	1.0944	0.0808	1.2049
EM9	0.0298	1.0861	0.0276	1.1905
EM10	0.0416	1.0088	0.0382	1.1060
EM11	0.0029	0.9433	0.0025	1.0321
EM12	0.0066	0.7074	0.0095	0.7670
EM13	0.0573	0.7132	0.0450	0.7405
EM14	0.0405	0.4206	0.0334	0.4597
EM15	0.0452	0.3026	/	/

properties when G16 is replaced by the wind farms of PMSG type and DFIG type, respectively.

It can be seen from Table 4 that when G16 is replaced by the wind farm of PMSG type, there exist 15 EM oscillatory modes consisting of 13 local modes (0.7-2.5Hz) and 2 interarea modes (0.2-0.7Hz). When G16 is replaced by the wind farm of DFIG type, there exist 14 EM oscillatory modes consisting of 13 local modes and 1 interarea mode.

Table 5 shows the most relevant generators and the corresponding mode shapes when G16 is replaced by PMSG and DFIG, respectively.

From Table 5, when G16 is replaced by the wind farm of PMSG type, the mode shape of EM15 represents a kind of special characteristics. In this EM mode, the magnitudes and angles of right eigenvectors with respect to the generator electrical speed bear relatively small difference, and no typical oscillations among generators can be found.

In the following studies, G14 is replaced by the wind farm consisting of 357 5MW PMSGs to specifically investigate the impacts of wind generation uncertainty and volatility on SSS via applying Monte Carlo method. Fig. 4 illustrates the Weibull frequency distribution histogram based on Monte Carlo with 6000 sample size.

Table 5. The most relevant generators and mode shapes when substituting for G16 in scenario 1

No.	G16 replaced by PMSG		G16 replaced by DFIG	
	Most relevant generator	Mode shape	Most relevant generator	Mode shape
EM1	G11	G11vsG13	G11	G11vsG13
EM2	G1	G1vsG8	G1	G1vsG8
EM3	G4	G4vsG7	G4	G4vsG7
EM4	G7	G4,G7vsG6	G7	G4,G7vsG6
EM5	G10	G1,G8vsG10	G10	G1,G8vsG10
EM6	G10	G1,G10, G8vsG9,G13	G10	G1,G10,G8vsG9, G13
EM7	G2	G2vsG3	G2	G2vsG3
EM8	G5	G5vsG6	G5	G5vsG6
EM9	G12	G13vsG12	G12	G13vsG12
EM10	G2	G2,G3vsG5,G6, G13	G2	G2,G3vsG5, G6,G13
EM11	G9	G9vsG2-G7	G9	G9vsG2-G7
EM12	G13	G12, G13vsG1-G9	G13	G12-G14vsG15
EM13	G15	G14vsG15	G14	G14vsG15
EM14	G14	G14,G15vsG13	G14	G14,G15vsG13
EM15	G14	-*	/	/

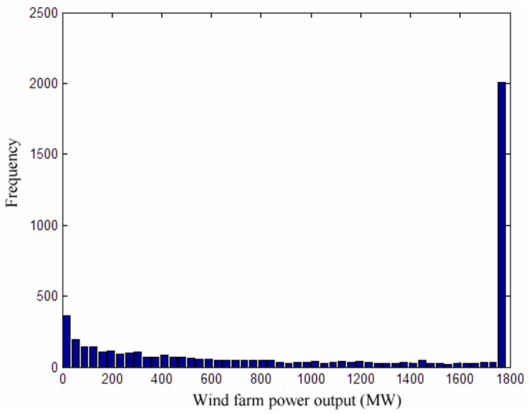

Fig. 7. Frequency distribution of wind farm power output

With combination of (24), we can obtain the frequency distribution of power output of wind farm as shown in Fig. 7. From Fig. 7, two concentrations of probability masses can be found in the distribution. The left concentration with zero power output corresponds to the situation in which the wind farm is cut off with a probability of 6.22% (373/6000). The right concentration with the maximum power output corresponds to the situation in which the wind farm generates the rated power with a probability of 39.63% (2378/6000).

The distribution of calculated eigenvalues within the specific dimensions: real axis [-100,100] and imaginary axis [-200,200] based on the pre-set samples is given in Fig. 8. In Fig. 8, in accordance with the statistical results, the stable probability of the test is 49.28% (2957/6000). Fig. 9 shows the distributions of picked out total 15 EM oscillatory modes on the complex plane. It should be noted that if the wind farm is cut off (373 samples), the EM oscillatory mode EM14 does not exist. It can be seen from Fig. 9 that in the 5627 simulations with wind farm connected, except EM15, the remaining EM oscillatory

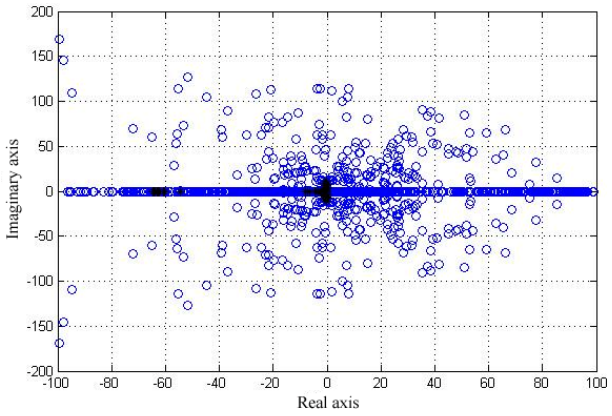

Fig. 8. Distribution of eigenvalues within specific dimensions in scenario 1

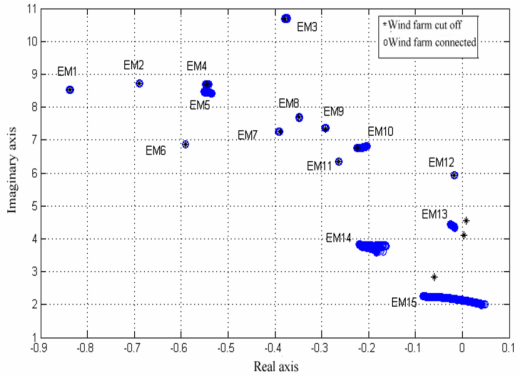

Fig. 9. Distributions of EM oscillatory modes in scenario 1

Table 6. The statistical features of all EM oscillatory modes in scenario 1

No.	Damping ratio		Oscillation Frequency		Most relevant gen.	Stable prob.
	Mean	Std	Mean	Std		
EM1	0.0352	2.45e-4	1.7016	8.2e-4	G11	100%
EM2	0.0789	5.53e-5	1.386	6.15e-5	G4	100%
EM3	0.0626	3.27e-4	1.358	1.55e-4	G1	100%
EM4	0.0978	8.51e-5	1.3567	6.52e-5	G7	100%
EM5	0.0642	7.89e-4	1.344	0.0025	G16	100%
EM6	0.0452	8.18e-5	1.2228	2.24e-4	G10	100%
EM7	0.0398	1.78e-4	1.1716	3.11e-4	G10	100%
EM8	0.0538	1.47e-4	1.1537	6.07e-4	G2	100%
EM9	0.0856	5.58e-5	1.0944	5.09e-5	G5	100%
EM10	0.0309	0.0013	1.0818	0.0042	G12	100%
EM11	0.0416	6.42e-5	1.0086	1.26e-4	G2	100%
EM12	0.0029	5.86e-5	0.9433	5.39e-5	G9	100%
EM13	0.0051	8.64e-4	0.7008	0.006	G13	100%
EM14*	0.0568	0.0014	0.6059	0.0054	G15	100%
EM15	0.0178	0.0208	0.3474	0.012	G13	67.63%

* Only for the situation of wind farm connected

modes EM1-EM14 fall into the left half complex plane (stable area). The stable probability for EM15 is 67.63% (4058/6000). In these two situations, the changes of EM1-EM4, EM6-EM9 and EM11-EM12 are relatively small.

Table 6 lists the statistical features of all EM oscillatory modes. From Table 6, it can be seen that the standard deviations in frequency with respect to EM5, EM10, EM13, EM14 and EM15 are relatively large, which denote that these oscillatory models are liable to be influenced by the wind speed.

4.2 Scenario 2: Grid connected directly

In this scenario, a wind farm consisting of 80 with single 5MW capacity PMSGs and a wind farm consisting of 200 with single 2MW capacity DFIGs are successively connected to the non-generator bus (bus 1-52), respectively. We found from the simulation results that when the wind farm of DFIG type is connected to bus 42, there exists an EM oscillatory mode with positive real part 0.0013±j3.5. When connecting to the remaining non-generator buses, the test system is small signal stable. For the wind farm of PMSG type, whichever non-generator bus is connected, the test system is small signal unstable. Similarly, the wind farm whatever is equipped with PMSG type or DFIG type does not participate in any EM oscillations. Table 7 gives the solved EM oscillatory modes and their properties when the wind farms of PMSG type and DFIG type are connected to bus 40 as shown in Fig. 6, respectively.

From Table 7, it can be found that when the wind farm of DFIG type is connected to bus 40, there exist 14 EM oscillatory modes, which is same as the number given in scenario 1. When the wind farm of PMSG type is connected to bus 40, there exist 16 EM oscillatory modes. Especially, there are 3 EM modes with negative damping ration, i.e. the integration of wind farm of PMSG type

Table 7. The EM oscillatory properties when connecting to bus 40 in scenario 2

No.	Bus 40 connected by PMSG		Bus 40 connected by DFIG	
	Damping ratio	Oscillation frequency	Damping ratio	Oscillation frequency
EM1	0.0403	1.8458	0.0360	1.6985
EM2	0.1124	1.7891	0.0638	1.3845
EM3	0.1110	1.7735	0.0791	1.3862
EM4	0.0912	1.3852	0.0981	1.3570
EM5	0.0574	1.3069	0.0454	1.2236
EM6	0.0590	1.3090	0.0405	1.1717
EM7	0.1079	1.2711	0.0543	1.1557
EM8	0.0316	1.2085	0.0858	1.0943
EM9	-0.1285	1.0417	0.0293	1.0909
EM10	0.0375	1.0666	0.0417	1.0089
EM11	0.0693	1.0733	0.0030	0.9432
EM12	0.1604	1.0184	0.0336	0.7595
EM13	0.0161	0.9857	0.0113	0.7087
EM14	0.0085	0.8938	0.0028	0.5721
EM15	-0.0017	0.8488	0.0337	0.4182
EM16	-0.0728	0.6371	/	/

Table 8. The most relevant generators and mode shapes when connecting to bus 40 in scenario 2

No.	Bus 40 connected by PMSG		Bus 40 connected by DFIG	
	Most relevant generator	Mode shape	Most relevant generator	Mode shape
EM1	G11	G11-G13vsG15	G11	G11vsG13
EM2	G15	G14,G15vsG13	G1	G1vsG8
EM3	G14	G14vsG15	G4	G4vsG7
EM4	G4	G4-G7vsG11	G7	G4,G7vsG6
EM5	G6	G4,G5vsG6,G7	G10	G1,G8vsG10
EM6	G8	G1-G3, G8vsG4,G5	G10	G1,G10, G8vsG9,G13
EM7	G16	G15vsG16	G2	G2vsG3
EM8	G9	G1vsG9	G5	G5vsG6
EM9	G13	G12vsG13	G12	G13vsG12
EM10	G13	G12vsG13	G2	G2,G3vsG5, G6,G13
EM11	G3	G2-G4,G13vsG1, G5,G6	G9	G9vsG2-G7
EM12	G5	G3,G5vsG4	G15	G15vsG14,G16
EM13	G10	G10,G13vsG12	G13	G12-G14vsG15
EM14	G1	G1vsG8,G10	G16	G14vsG16
EM15	G7	G6vsG7	G15	G12,G13vsG14, G15
EM16	G2	G2vsG3	/	/

leads to a worsening of system damping. The most relevant generators pertinent to the EM modes and the mode shapes are summarized in Table 8.

From Table 8, compared with the results given in scenario 1, the relatively big changes in the most relevant generators and the mode shapes happened when the wind farm equipped with PMSG or DFIG is connected to a specific non-generator bus. In summary, in accordance with the aforementioned simulation results, it is more suitable for the wind farm of DFIG type than the wind farm of PMSG type to be connected to the power grid directly.

In the succedent simulation studies, we mainly focus on the impacts of wind generation uncertainty and volatility

on SSS via applying Monte Carlo method when the wind farm of PMSG type is connected to bus 40. The sample size for Monte Carlo simulation is set to be 5000.

Similarly, for the frequency distribution of wind farm power output, the left concentration with respect to the wind farm cut off is happened in a probability of 6.4% (320/5000); the right concentration with respect to the rated power output of wind farm is happened in a probability of 40.12% (2006/5000).

The distribution of calculated eigenvalues within the specific dimensions: real axis [-10, 10] and imaginary axis [-10,10] based on the pre-set samples is given in Fig. 10. It can be seen from Fig. 10 that some eigenvalues are located in the right half complex plane, i.e. the small signal stability is unstable.

According to the simulation analysis, total 16 EM oscillatory modes are identified. Fig. 11 illustrates the distributions of these EM oscillatory modes. Similarly, if the wind farm is cut off (320 samples), the EM oscillatory mode EM16 does not exist. In this situation, there exist only 15 EM oscillatory modes, which all fall into the left half complex plane. When the wind farm is connected (total 4680 samples) to the power grid, EM14 and EM16 fall into the right half complex plane with the probability

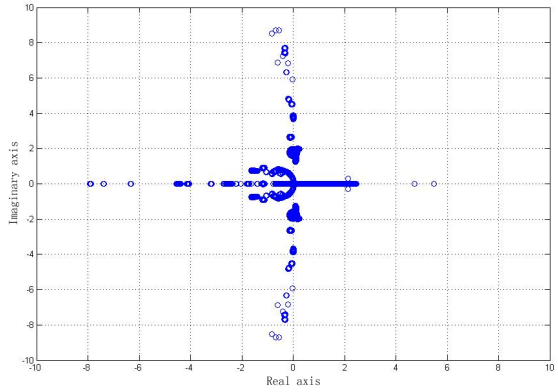

Fig. 10. Distribution of eigenvalues within specific dimensions in scenario 2

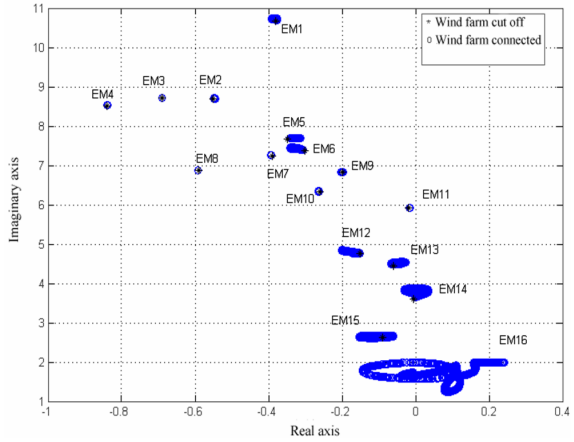

Fig. 11. Distributions of EM oscillatory modes in scenario 2

Table 9. The statistical features of all EM oscillatory modes in scenario 2

No.	Damping ratio		Oscillation Frequency		Most relevant gen.	Stable prob.
	Mean	Std	Mean	Std		
EM1	0.0356	2.17e-4	1.7074	0.0015	G11	100%
EM2	0.079	1.82e-5	1.3861	2.20e-5	G4	100%
EM3	0.0628	8.70e-5	1.3851	1.06e-4	G1	100%
EM4	0.0979	2.28e-5	1.3568	1.81e-5	G7	100%
EM5	0.0421	8.37e-4	1.2245	5.29e-4	G10	100%
EM6	0.0438	8.30e-4	1.1831	0.0023	G10 36.62% G8 64.38%	100%
EM7	0.0541	5.39e-5	1.1546	2.32e-4	G2	100%
EM8	0.0857	1.93e-5	1.0944	1.55e-5	G5	100%
EM9	0.0294	2.34e-4	1.0876	0.001	G12	100%
EM10	0.0416	4.35e-5	1.0092	1.27e-4	G2	100%
EM11	0.0028	3.24e-5	0.9433	2.84e-5	G9	100%
EM12	0.0392	0.002	0.7679	0.0032	G15	100%
EM13	0.008	0.0025	0.7189	0.0024	G13	100%
EM14	-0.0016	0.0037	0.6092	0.0085	G16	27.26%
EM15	0.0277	0.005	0.4234	0.0022	G14 95.85% G15 1.39% G13 2.76%	100%
EM16*	-0.0702	0.0544	0.2910	0.0303	G15	17.42%

* Only for the situation of wind farm connected

of 72.74% (3637/5000) and 82.58% (4129/5000), respectively. The remaining EM oscillatory modes are all located in the left half complex plane. In these two situations, the changes of EM1-EM4 and EM7-EM11 are relatively small. The change of EM16 is relatively remarkable.

The characteristics of EM oscillatory modes involving damping ratio, oscillation frequency etc., are given in Table 9. From Table 9, it can be seen that these EM oscillatory modes from EM12 to EM16 are liable to be influenced by the wind speed. It should be noted that for EM6 and EM15, there exists a certain uncertainty for the most relevant generator. For example, EM6 is most relevant to G10 with a probability of 36.62%, and to G8 with a probability of 64.38%. The similar phenomenon is happened to EM15.

5. Conclusion

With large scale integration of wind power, how to evaluate the effects of wind power uncertainty and volatility on power system dynamics, especially on small signal stability is posing great challenges for the electrical engineers and scientists. In this paper, based on the modeling of wind farm equipped with PMSG, two scenarios involving the replacement of traditional synchronous generator with wind farm and direct connection of wind farm are designed and studied for the

IEEE 16-generator-68-bus test system. From the simulation results, it can be found that there exist two concentrations for the distribution of wind farm power output due to the uncertainties of wind speed. And the probability of keeping test system stable is determined by some eigenvalues or wind speed conditions. Furthermore, the statistical analysis for the EM oscillatory modes further shows the effects of wind power uncertainty on power system small signal stability.

Acknowledgements

This work was supported in part by the State Grid Corporation of China Science & Technology project 'Research on the grid connection experimental test and assessment technology for the high altitude and portable large capacity wind power generation', by State Grid Corporation of China under the contract State Grid Research 304(2013), the Research Project of Science and Technology from Shenzhen Development and Innovation Committee (ZDSY20120619141142918).

References

[1] A . Thomas , Wind Power in Power Systems: Chichester, 2005, pp. 523-553.

[2] F. Mei, B. C. Pal, "Modelling and Small-Signal Analysis of a Grid Connected Doubly-Fed Induction Generator," in Proceedings of IEEE Power Engineering Society General Meeting, San Francisco, CA, New York, USA, 2005.

[3] F. Wu, X. P. Zhang, K. Godfrey, P. Ju, "Modeling and Control of Wind Turbine with Doubly Fed Induction Generator," in Proceedings of IEEE Power Systems Conference and Exposition, Atlanta, Georgia, USA, 2006.

[4] G. Durga, V. Vittal, H. Terry, "Impact of Increased Penetration of DFIG-Based Wind Turbine Generators on Transient and Small Signal Stability of Power Systems," IEEE Trans. Power Systems, vol.24, no.3, pp.1426-1434, Aug. 2009.

[5] L. B. Shi, C. Wang, L. Z. Yao, L. M. Wang, Y. X. Ni, "Analysis of Impact of Grid-connected Wind Power on Small Signal Stability," Wind Energy, vol.14, no.4, pp.517-537, May 2011.

[6] H. Espen, Ian Norheim, Kjetil Uhlen, "Large Scale Wind Power Integration in Norway and Impact on Damping in the Nordic Grid," Wind Energy, vol. 8, no. 3, pp.375-384, July/Sep. 2005.

[7] Wu F., Zhang X. P., Ju P., "Small Signal Stability Analysis and Control of the Wind Turbine with the Direct-drive Permanent Magnet Generator Integrated to the Grid," Electric Power Systems Research, vol. 79, no. 12, pp.1661-1667, Dec. 2009.

[8] L. Kang, L. B. Shi, Y. X. Ni, L. Z. Yao, B. Masoud, "Small Signal Stability Analysis with Penetration of Grid-connected Wind Farm of PMSG Type," in Proceedings of the International Conference on Advanced Power System Automation and Protection, Beijing, China, 2011.

[9] T. Knuppel, J. N. Nielsen, K. H. Jensen, A. Dixon, J. Ostergaard, "Small-signal stability of wind power system with full-load converter interfaced wind turbines," IET Renewable Power Generation, vol.6, no.2, pp. 79-91, Mar. 2012.

[10] S. Q. Bu, W. Du, H. F. Wang, Z. Chen, L. Y. Xiao, H. F. Li, "Probabilistic analysis of small-signal stability of large-scale power systems as affected by penetration of wind generation," IEEE Trans. Power Systems, vol.27, no.2, pp.762-770, May 2012.

[11] H. Huang, C. Mao, J. Lu, D. Wang, "Small-signal modelling and analysis of wind turbine with direct drive permanent magnet synchronous generator connected to power grid," IET Renewable Power Generation, vol.6, no.1, pp. 48-58, Jan. 2012.

[12] H. Z. Huang, C. Y. Chung, K. W. Chan, H. Y. Chen, "Quasi-Monte Carlo based probabilistic small signal stability analysis for power systems with plug-in electric vehicle and wind power integration," IEEE Trans. Power Systems, vol.28, no.3, pp.3335-3343, 2013.

[13] M. Jafarian, A. M. Ranjbar, "Interaction of the dynamics of doubly fed wind generators with power system electromechanical oscillations," IET Renewable Power Generation, vol.7, no.2, pp. 89-97, Mar. 2013.

[14] Koch F., Gresch M., Shewarega F., Erlich I., Bachmann U., "Consideration of Wind Farm Wake Effect in Power System Dynamic Simulation," in Proceedings of the IEEE Power Tech Conference, Russia, 2005.

[15] Gerardo Tapia, Arantxa Tapia, J. Ostolaza Xabier, "Two Alternative Modeling Approaches for the Evaluation of Wind Farm Active and Reactive Power Performances," IEEE Trans. on Energy Conversion, vol.21, no.4, pp. 909-920, Dec. 2006.

[16] Prabha Kundur, Power System Stability and Control: New York: McGraw-Hill, 1994, pp. 699-826.

[17] G. J. Bowden, P. R. Barker, V. O. Shestopal, T. W. Twidell, "The Weibull Distribution Function and Wind Power Statistics," Wind Engineering, vol.7, no.2, pp. 85-98, 1983.

[18] Pal Bikash, Chaudhuri Balarko, Robust Control in Power Systems: Springer, 2005, pp. 39-43.

Li-Bao Shi He received Ph.D. degree in Electrical Engineering from Chongqing University, China, in 2000. His research interests are wind power in power systems, power system restoration control, computational intelligence in power system optimal operation and control, EMS/DMS, and power system stability analysis.

Li Kang She received B.S degree in Electrical Engineering from Tsinghua University, China, in 2009. Her research interests are wind power in power systems.

Liang-Zhong Yao He received the PhD degree in 1993 in electrical power system engineering from Tsinghua University, China. He is currently the Vice President of State Grid Electric Power Research Institute, China. His research interests are wind power in power systems.

Shi-Yao Qin He received master degree in TaiYuan University of Science and Technology in 2003. His research interests are wind power simulation, planning, test technology.

Rui-Ming Wang He received master degree in North China Electric Power University in 2003. His research interests are wind power simulation, planning, test technology.

Jin-Ping Zhang He received master degree in HuaZhong University of Science and Technology in 2000. His research interests are wind farm and wind turbine test technology.